



## Advantages of stainless steel sieves as support for catalytic N<sub>2</sub>O decomposition over K-doped Co<sub>3</sub>O<sub>4</sub>



Anna Klyushina<sup>a</sup>, Kateřina Pacultová<sup>a</sup>, Stanislava Krejčová<sup>b</sup>, Grzegorz Słowik<sup>c</sup>, Květuše Jiráková<sup>d</sup>, František Kovanda<sup>b</sup>, Janusz Ryczkowski<sup>c</sup>, Lucie Obalová<sup>a,d,\*</sup>

<sup>a</sup> Institute of Environmental Technology, Faculty of Metallurgy and Materials Engineering, VŠB - Technical University of Ostrava, 17. listopadu 15/2172, Ostrava, Czech Republic

<sup>b</sup> Institute of Chemical Technology, Prague, Technická 5, Prague, Czech Republic

<sup>c</sup> Maria Curie-Skłodowska University, Faculty of Chemistry, Pl. M. Curie-Skłodowskiej 3/402, Lublin, Poland

<sup>d</sup> Institute of Chemical Process Fundamentals of the ASCR, Rozvojová 135, Prague, Czech Republic

### ARTICLE INFO

#### Article history:

Received 2 November 2014

Received in revised form 7 May 2015

Accepted 12 May 2015

Available online 16 June 2015

#### Keywords:

N<sub>2</sub>O catalytic decomposition

Potassium promoter

Co<sub>3</sub>O<sub>4</sub>

TiO<sub>2</sub> support

Stainless steel support

### ABSTRACT

Supported Co<sub>3</sub>O<sub>4</sub> catalysts were prepared by heating of the cobalt hydroxide synthesized electrochemically on stainless steel sieves and by heating of the commercial TiO<sub>2</sub> pellets impregnated with cobalt nitrate solution; the catalysts were modified with potassium promoter. For comparison, the grained K-doped Co<sub>3</sub>O<sub>4</sub> catalyst was prepared from the precipitated precursor. The catalysts were characterized by AAS, XRD, N<sub>2</sub> physisorption, TPR-H<sub>2</sub>, STEM and SEM and tested in N<sub>2</sub>O catalytic decomposition in laboratory conditions. Mathematic model based on ideal plug flow and laboratory kinetic data was used to compare catalytic performance of unit bed volume of both K-Co<sub>3</sub>O<sub>4</sub> supported catalysts. Simulation results showed that higher conversions in potential large scale application can be achieved over the catalyst deposited on stainless steel sieves in comparison with TiO<sub>2</sub> pellets. K/Co<sub>3</sub>O<sub>4</sub> stainless steel wire mesh catalyst combines suitable features of active cobalt species with the effective utilization of all present active components.

© 2015 Elsevier B.V. All rights reserved.

### 1. Introduction

Nitrous oxide (N<sub>2</sub>O) has a high global warming potential (310 times higher than CO<sub>2</sub>) and contributes to the destruction of stratospheric ozone. The largest amounts of N<sub>2</sub>O emitted from anthropogenic sources are connected with agricultural activity but reduction of these emissions is very problematic. The largest industrial sources of N<sub>2</sub>O emissions are waste gases from nitric acid production plants (globally 400 kt N<sub>2</sub>O per year) [1]. The low-temperature catalytic decomposition of N<sub>2</sub>O (up to 450 °C) to nitrogen and oxygen offers attractive solution for decreasing N<sub>2</sub>O emissions in tail gas from nitric acid production plants.

Among a large number of catalysts tested for the decomposition of N<sub>2</sub>O, cobalt spinels presented excellent catalytic activities which makes them promising for practical application in abatement of N<sub>2</sub>O emitted in waste gases from HNO<sub>3</sub> production plants

[2–4]. The most common cobalt oxide-based catalyst (Co<sub>3</sub>O<sub>4</sub> spinel) is sufficiently stable and does not exhibit inhibition effect caused by oxygen accumulation on its surface during reaction at lower temperatures (300 °C) [5]. Modification of the cobalt spinels with small amounts of alkali metals significantly increases the activity of the catalyst [3–7]. These promoters, especially potassium, increase an electron density of Co<sup>2+</sup> and make it more readily to donate electrons to the molecule of N<sub>2</sub>O and thus facilitate the activation of N<sub>2</sub>O and its scission. Moreover, potassium doping also promote the reduction of Co<sup>3+</sup> to Co<sup>2+</sup> through an electron donation effect; therefore promote the desorption of oxygen from catalysts surface, i.e., the controlling step of N<sub>2</sub>O decomposition is favored [5].

To the best of our knowledge, only two research groups reported on manufacturing of shaped cobalt spinel based catalysts in pilot plant scale conditions [6,8,9]. In both cases, the conventional packed beds with pelletized cobalt spinel based catalysts were used for N<sub>2</sub>O decomposition. However, some problems can be connected with production and application of the pelletized mixed oxides as the pelletized catalysts generally show: (i) troubles accompanying formation of the precursors into larger pellets (5–8 mm), (ii) relatively low mechanical strength, (iii) high pressure drop, and (iv) low utilization of the whole pellet volume due to fact that the

\* Corresponding author at: Institute of Environmental Technology, Faculty of Metallurgy and Materials Engineering, VŠB - Technical University of Ostrava, 17. listopadu 15/2172, Ostrava, Czech Republic. Tel.: +420 597327300.

E-mail address: [Lucie.obalova@vsb.cz](mailto:Lucie.obalova@vsb.cz) (L. Obalová).

## Nomenclature

$A_f$	surface of holes in the sieve ( $m^2$ )
$A_p$	surface of sieve ( $m^2$ )
$C$	coefficient $C=f(\text{Re}, t/D)$ , $C \approx 0.98$ for $t/D > 1.6$ ; $\text{Re} > 4000$
$C_A$	concentration of component A ( $\text{N}_2\text{O}$ ) ( $\text{mol m}^{-3}$ )
$C_{A0}$	initial concentration of component A ( $\text{N}_2\text{O}$ ) ( $\text{mol m}^{-3}$ )
$C_D$	coefficient of resistance (-)
$D$	diameter of holes in the sieve (m)
$D_{\text{eff}}$	effective diffusion coefficient ( $\text{m}^2 \text{s}^{-1}$ )
$D$	overall diffusivity ( $\text{m}^2 \text{s}^{-1}$ )
$D_k$	Knudsen diffusivity ( $\text{m}^2 \text{s}^{-1}$ )
$D_{ij}$	binary diffusion coefficient of molecular diffusivity ( $\text{m}^2 \text{s}^{-1}$ )
$d_p$	catalyst particle diameter (m)
$E_a$	activation energy (J/mol)
$g_c$	sphericity of catalyst particle (-)
$k$	kinetic constant, 1st order rate law ( $\text{m}^3 \text{s}^{-1} \text{kg}^{-1}$ )
$k_c$	mass transfer coefficient ( $\text{m s}^{-1}$ )
$k_0$	pre-exponential factor
$m$	catalyst weight (g)
$M_i$	molar weight of compound $i$ ( $\text{g mol}^{-1}$ )
$n$	number of the sieves in pilot plant reactor
$p$	pressure at the reactor outlet (Pa)
$p_{\text{atm}}$	atmospheric pressure (Pa)
$p_0$	pressure at the reactor inlet (Pa)
$\Delta p$	pressure drop (Pa)
$q$	tortuosity
$R$	universal gas constant ( $\text{J mol}^{-1} \text{K}^{-1}$ )
$r$	reaction rate per unit volume of catalyst bed ( $\text{mol m}^{-3} \text{s}^{-1}$ )
$r_o$	catalyst pore radius (m)
$r_p$	catalyst particles radius (m)
$S$	cross section of reactor ( $\text{m}^2$ )
$T$	standard temperature (293.15 K)
$t$	thickness of sieve (m)
$V$	volume of the catalyst bed ( $\text{m}^3$ )
$\dot{V}$	total volumetric flow ( $\text{m}^3 \text{s}^{-1}$ )
$v$	superficial velocity ( $\text{m s}^{-1}$ )
$(\Sigma v)_i$	diffusion volume
$w_{\text{Co}}$	mass fraction of Co in the catalyst (-)
$X_A$	conversion of component A ( $\text{N}_2\text{O}$ )
$X_{\text{N}_2\text{O}}$	molar fraction of $\text{N}_2\text{O}$ entering the reactor (-)
$X_{\text{N}_2\text{O}}$	conversion of $\text{N}_2\text{O}$ (-)
$z$	axial coordinate (m)

### Greek symbols

$\alpha_i$	stoichiometric coefficient of component $i$ ( $\text{N}_2\text{O}$ )
$\varepsilon_p$	porosity of catalyst particle
$\varphi$	porosity of catalyst bed (-)
$\Phi$	Thiele modul
$\mu$	dynamic viscosity of gas (Pa s)
$\eta$	internal effectiveness factor
$\rho$	density of gas ( $\text{kg m}^{-3}$ )
$\rho_b$	bulk density of the catalyst bed ( $\text{kg m}^{-3}$ )
$\rho_c$	bulk density of the catalyst ( $\text{kg m}^{-3}$ )

catalytic reaction proceeds only on the surface of pores while active species which are not present on surface are unutilized. Moreover, hindering effect of internal diffusion causes that the catalytic reaction can take place only in a narrow surface region of the shaped catalysts.

Deposition of active phase on suitable support can solve problem with formation of shaped oxide catalysts and their low mechanical strength. Moreover, better utilization of active phase is achieved by applying of a thin active layer deposited on the inactive support material. The most common supports are high surface area supports like different type of  $\text{Al}_2\text{O}_3$ ,  $\text{TiO}_2$ ,  $\text{SiO}_2$  etc. By optimization of their porous structure and shapes, the hindering effect of internal diffusion can be decreased. Recently, stainless steel wire-mesh (SSWM) supported metal oxide catalysts have been published as a very promising structured catalytic system. Although the mesh is almost non-porous with generally very low specific surface area, it provides high geometric surface area for supporting the active components and allows deposition of large amount of active components per catalysts volume. The SSWM-supported catalysts are also sufficiently flexible to be fit into any kind of reactor, while ensuring a low pressure drop and good heat transfer [10]. Recently, the stainless steel wire mesh was also employed as support for potassium-doped  $\text{Co}_3\text{O}_4$  nanowires and tested for  $\text{N}_2\text{O}$  decomposition [5]. The activity of this novel structured catalyst was compared with reported results obtained on grains of cobalt-containing catalysts. Due to a different reactor concept and operation conditions, the kinetic constants were used for comparison with literature data. Based on this comparison, stainless steel wire mesh-supported potassium-doped cobalt oxide had the highest value of kinetic constant.

However, from practical point of view, comparison of  $\text{N}_2\text{O}$  conversions obtained over the unit volume of catalyst bed rather than comparison based on the kinetics constants or unit weight of catalysts gives better picture about efficiency of catalysts with different shapes.

The subject of presented work was to compare catalytic performance of active phase (potassium-promoted  $\text{Co}_3\text{O}_4$ ) supported on low surface area support to avoid internal diffusion limitation effects and porous commonly used support with high surface area which enables distribution of high amount of active species. Stainless steel wire-mesh was chosen as nonporous low surface area support while commercial  $\text{TiO}_2$  tablets were used as porous high surface area support. The aim was to show, how much the utilization of the active species can be influenced by the choice of support. The prepared catalysts were characterized by various methods and tested for  $\text{N}_2\text{O}$  catalytic decomposition. The obtained results were compared with the potassium-promoted  $\text{Co}_3\text{O}_4$  catalyst in the form of grains. For comparison of catalytic performance, the  $\text{N}_2\text{O}$  conversions which could be achieved over the unit volume of catalyst bed were calculated using simple pseudo one dimensional model of ideal plug flow reactor.

## 2. Experimental

### 2.1. Preparation of catalysts

#### 2.1.1. Potassium-promoted $\text{Co}_3\text{O}_4$ deposited on stainless steel sieves

The K-modified  $\text{Co}_3\text{O}_4$  was prepared by thermal decomposition of cobalt hydroxide precursor obtained by electrochemical synthesis on the stainless steel; the stainless steel sieve (71% Fe, 16% Cr, 11% Ni, 2% Mo) with a mesh size of  $40 \mu\text{m}$  was used as a support. The electrochemical deposition of precursor was performed in aqueous solution of cobalt nitrate in the presence of  $\text{KNO}_3$  as supporting electrolyte. The potentiostatic mode in a single compartment, three-electrode cell was applied; the stainless steel sieve was used as the working electrode, the Pt foil was used as counter electrode and the potential was measured with respect to an aqueous saturated calomel electrode (SCE). Based on former experiments carried out under various conditions, the following parameters

were chosen:  $\text{Co}(\text{NO}_3)_2$  concentration  $0.10 \text{ mol l}^{-1}$ ,  $\text{KNO}_3$  concentration  $0.25 \text{ mol l}^{-1}$ , potential  $-1.15 \text{ V}$  vs. SCE, temperature  $30^\circ\text{C}$ , and deposition time 1200 s. The washed sample was dried at  $60^\circ\text{C}$  and calcined at  $500^\circ\text{C}$  for 4 h in air to obtain the supported oxide catalyst. Before the catalytic measurements, the calcined sample was cut into pieces of about  $4 \text{ mm} \times 4 \text{ mm}$ . The catalyst was labeled as  $\text{K}/\text{Co}_3\text{O}_4/\text{SSWM}$ .

#### 2.1.2. Potassium-promoted $\text{Co}_3\text{O}_4$ deposited on $\text{TiO}_2$ pellets

The K-modified  $\text{Co}_3\text{O}_4$  supported on  $\text{TiO}_2$  was prepared by incipient wetness impregnation of the commercial  $\text{TiO}_2$  pellets (Eurosupport, Czech Republic, anatase, surface area  $200 \text{ m}^2 \text{ g}^{-1}$ ) with an aqueous solution of mixed salts  $\text{Co}(\text{NO}_3)_2$  and  $\text{K}_2\text{CO}_3$  heated to  $60^\circ\text{C}$ . Impregnation was followed by drying at  $105^\circ\text{C}$  for 3 h and calcined at  $500^\circ\text{C}$  for 4 h in air. The catalyst was labeled as  $\text{K}/\text{Co}_3\text{O}_4/\text{TiO}_2$  pellets.

#### 2.1.3. Potassium-promoted $\text{Co}_3\text{O}_4$ in the form of grains

The  $\text{Co}_3\text{O}_4$  was prepared by calcination of cobalt hydroxide precursor obtained by precipitation of cobalt nitrate. An aqueous solution (140 ml) of  $\text{Co}(\text{NO}_3)_2$  ( $2.0 \text{ mol l}^{-1}$ ) was quickly added to 700 ml of NaOH aqueous solution ( $0.80 \text{ mol l}^{-1}$ ). The resulting suspension was vigorously stirred and bubbled with air at room temperature for 5 min. Then the product was filtered off, thoroughly washed with distilled water, dried at  $30^\circ\text{C}$ , and calcined at  $500^\circ\text{C}$  for 4 h in air. The calcined sample was crushed and sieved to obtain a fraction with particle size of  $0.160\text{--}0.315 \text{ mm}$ . Prepared oxide was mixed with solution of  $\text{KNO}_3$ , dried at  $105^\circ\text{C}$ ; and calcined at  $500^\circ\text{C}$  for 4 h in air. The calcined sample was crushed and sieved again to obtain a fraction with particle size of  $0.160\text{--}0.315 \text{ mm}$ . The catalyst was labeled as  $\text{K}/\text{Co}_3\text{O}_4$  grains.

### 2.2. Characterization of the samples

The chemical composition of the prepared catalysts was determined by atomic absorption spectroscopy (AAS) method using a Spectr AA880 instrument (Varian) after dissolving the samples in hydrochloric acid.

The powder X-ray diffraction (XRD) patterns were recorded with  $\text{CoK}\alpha$  irradiation ( $\lambda = 1.789 \text{ \AA}$ ) using the Bruker D8 Advance diffractometer (Bruker AXS) equipped with a fast position sensitive detector VANTEC 1. Measurements were carried out in the reflection mode, powdered samples were pressed in a rotational holder and goniometer with the Bragg-Brentano geometry in  $2\theta$  range from  $15^\circ$  to  $80^\circ$  with step size  $0.02^\circ$  was used. The samples deposited on stainless steel sieves were measured as prepared. Phase composition was evaluated using database PDF 2 Release 2004 (International Centre for Diffraction Data). The crystallite size was calculated according to the (3 1 1)  $\text{Co}_3\text{O}_4$  spinel diffraction peak using the Scherrer formula; lanthanum hexaboride ( $\text{LaB}_6$ ) was used as a standard.

Surface areas of the catalysts in the form of pellets and grains were determined by  $\text{N}_2$  adsorption/desorption at  $-196^\circ\text{C}$  using ASAP 2010 instrument (Micromeritics, USA) and evaluated by BET method. Surface area of the catalyst in the form of sieve was determined by krypton adsorption/desorption at  $-197.5^\circ\text{C}$ . Prior to the measurements, the samples were dried at  $120^\circ\text{C}$  for at least 12 h. In addition, mercury porosimetry (Autopore 9600, Micromeritics, USA) was used for determination of catalyst pellets total pore volume and pore diameter.

Temperature programmed reduction (TPR- $\text{H}_2$ ) measurements of the calcined samples were performed using a system described in details in [11], with a  $\text{H}_2/\text{N}_2$  mixture (10 mol%  $\text{H}_2$ ), flow rate 50 ml/min and the linear temperature increase of  $20^\circ\text{C}/\text{min}$  up to  $1000^\circ\text{C}$ . Change in  $\text{H}_2$  concentration was detected with a mass spectrometer Omnistar 300 (Pfeiffer Vacuum).

The electron microscope Titan G2 60–300 kV FEI Company, equipped with: field emission gun (FEG), monochromator, three condenser lenses system, the objective lens system, image correction (Cs-corrector), HAADF detector and EDS spectrometer (Energy Dispersive X-Ray Spectroscopy) EDAX Company with detector Si(Li) was used to display the prepared catalysts. Microscopic studies of the catalysts were carried out at an accelerating voltage of the electron beam equal to 300 kV. The mapping was carried out in the STEM mode by collecting point by point EDS spectrum of each of the corresponding pixels in the map. Quantitative and qualitative distribution of individual elements in the catalyst was examined on the basis of three selected areas. In each of the areas two spectra were obtained. The first spectrum coming from the support fragment and the second spectrum coming from  $\text{Co}_3\text{O}_4$  active phase fragment were obtained in order to determine the potassium content in each phase.

### 2.3. Catalytic measurements

$\text{N}_2\text{O}$  catalytic decomposition was performed in integral fixed bed stainless steel reactors of 5.5 mm or 50 mm internal diameter in the temperature range from  $300$  to  $450^\circ\text{C}$  and at atmospheric pressure. The feed introduced to the reactor contained 0.1 mol%  $\text{N}_2\text{O}$  in  $\text{N}_2$ , the flow rate varied from 100 to 500 ml/min. The catalyst bed of powdered sample contained 0.3 g of the sample with particle size  $0.160\text{--}0.315 \text{ mm}$  and inert glass beads of the same fraction; the total flow rate was 300 ml/min and measurements were performed in reactor with diameter of 5.5 mm. The bed with tablets contained 10 ml (8.2 g) of the sample with particle size of 5 mm and inert Rashing rings of the same size, flow rate was 500 ml/min and reactor with 50 mm diameter was used. The bed of sieves contained 0.1 g of sample in the form of squares  $4 \text{ mm} \times 4 \text{ mm}$  and quartz wool; flow rate was 100 ml/min and reactor with 5.5 mm diameter was used. All tested catalysts were activated at  $450^\circ\text{C}$  in the flow of  $\text{N}_2$  for 1 h. For  $\text{N}_2\text{O}$  analysis IR analyzer (Sick) was used.

In both used reactors, the influence of external diffusion and axial dispersion on the  $\text{N}_2\text{O}$  conversion was studied previously [12]. The catalytic tests were done at the flow rates, where these two effects can be neglected, thus experimental data can be transferred from one reactor to another. A care was also taken to fulfill the sufficient total bed high (catalyst + inert) to obtain plug flow as described above.

## 3. Results and discussion

### 3.1. Characterization of the catalysts

Chemical composition, results of TPR- $\text{H}_2$  measurements, surface areas and the pore radius of the prepared catalyst are summarized in Table 1. It is obvious that samples differ significantly in the amount of active cobalt species. The highest cobalt content was found in the grained catalyst while the lowest in the  $\text{K}/\text{Co}_3\text{O}_4$  supported on sieves. Apart from active species, the samples also contained different amounts of potassium promoter (from 0.02 to 1.2 wt.%) leading to molar ratio of K/Co from 0.01 to 0.05.  $\text{K}/\text{Co}_3\text{O}_4/\text{TiO}_2$  in pellet form and  $\text{K}/\text{Co}_3\text{O}_4$  in grain form can also contain sodium residuals from preparation which could affect the activity of cobalt-spinel catalysts. Results showed that amount of Na in  $\text{K}/\text{Co}_3\text{O}_4/\text{TiO}_2$  pellets and in  $\text{K}/\text{Co}_3\text{O}_4$  grains was very low compared to amount of potassium in these samples (Na 0.05 wt.% in  $\text{K}/\text{Co}_3\text{O}_4$  grains and Na 0.18 wt.% in  $\text{K}/\text{Co}_3\text{O}_4/\text{TiO}_2$  pellets). Also number of sodium atoms per  $\text{nm}^2$  ( $0.6 \text{ at}/\text{nm}^2$  max) was eight times less than values applied for doping by alkali metals (approximately  $2 \text{ at}/\text{nm}^2$ ) [6,13]. Hence, influence of sodium presence on reaction rate can be considered as negligible.

**Table 1**  
Characterization results of prepared catalysts.

Sample	K/Co <sub>3</sub> O <sub>4</sub> /SSWM	K/Co <sub>3</sub> O <sub>4</sub> /TiO <sub>2</sub> _pellets	K/Co <sub>3</sub> O <sub>4</sub> _grains
Co (wt.%)	4.8	19.2	73.4
K (wt.%)	0.02	0.57	1.20
Na (wt.%)	n.d.	0.18	0.05
K/Co molar ratio	0.01	0.05	0.03
TPR 25–500 °C (mmol g <sup>-1</sup> )	1.3	3.9	17.6
TPR 25–500 °C (mol H <sub>2</sub> mol <sub>Co</sub> <sup>-1</sup> )	1.59	1.19	1.41
TPR-H <sub>2</sub> T <sub>max</sub> (°C)	362	422	312; 416
S <sub>BET</sub> (m <sup>2</sup> g <sup>-1</sup> )	0.99	75.3 <sup>a</sup>	12.4 <sup>a</sup>
Pore volume (cm <sup>3</sup> g <sup>-1</sup> )	n.d.	0.23 <sup>a</sup> ; 0.48 <sup>b</sup>	0.09 <sup>a</sup>
Pore radius r <sub>o</sub> (nm)	n.d.	5.1 <sup>a</sup> ; 41.2 <sup>b</sup>	18.0 <sup>a</sup>
Crystallite size (nm)	45	49	44

<sup>a</sup> From BET method  $r_o = 2V/A_{ads}$  ( $V$  = mesopore volume,  $A_{ads}$  = surface area determined from adsorption branch of N<sub>2</sub> sorption).

<sup>b</sup> From mercury porosimetry measurement, n.d. – not determined.

Powder XRD patterns of prepared catalysts are depicted in Fig. 1. The precipitation of cobalt nitrate with sodium hydroxide in aqueous solution resulted in formation of highly crystalline  $\beta$ -Co(OH)<sub>2</sub> (PDF #30-0443) – not shown. No other crystalline phases were found in the precipitated sample. During calcination at 500 °C in air the  $\beta$ -Co(OH)<sub>2</sub> was transformed into Co<sub>3</sub>O<sub>4</sub> oxide (PDF #80-1545); all diffraction lines found in the powder XRD pattern of the K/Co<sub>3</sub>O<sub>4</sub>\_grains sample were coincident with this oxide (Fig. 1, pattern (a)). The Co<sub>3</sub>O<sub>4</sub> oxide was identified also in the powder XRD pattern of the catalysts deposited on TiO<sub>2</sub> pellets, which were impregnated with cobalt nitrate solution and then calcined at 500 °C in air (K/Co<sub>3</sub>O<sub>4</sub>/TiO<sub>2</sub>\_pellets). Anatase from the support was also found in this sample, together with the Co<sub>3</sub>O<sub>4</sub> oxide (Fig. 1, pattern (b)).

Product with different phase composition was obtained by electrochemical synthesis of precursor on the stainless steel sieve. Cathodic reduction of nitrates in aqueous solutions results in generation of OH<sup>-</sup> anions and increasing pH at the working electrode, followed by precipitation of Co cations. The sample after electrochemical deposition showed broad diffraction peaks of relatively low intensity at about 14°, 39°, and 70° 2 $\theta$ , which can be ascribed to a hydroxalcalite-like phase (not shown). Partial oxidation of Co<sup>2+</sup> cations to Co<sup>3+</sup> and formation of Co(II)–Co(III) layered double hydroxide could be expected. Results reported by Xu and Zeng [14] indicated important role of OH/Co molar ratio during synthesis of cobalt hydroxides: High initial OH/Co molar ratio facilitates formation of  $\beta$ -Co(OH)<sub>2</sub> whereas application of low initial OH/Co molar ratios resulted in formation of Co(II)–Co(III) hydroxalcalite-like

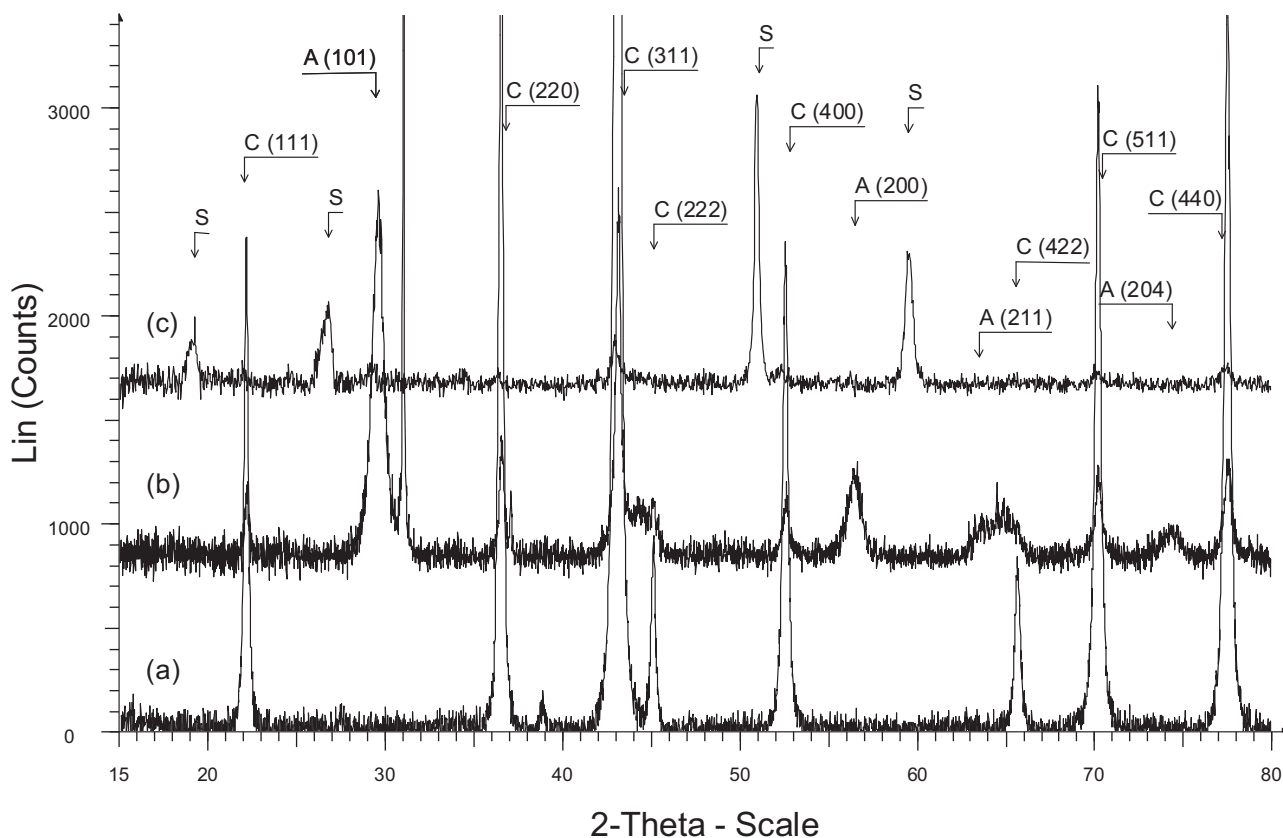


**Fig. 1.** Powder XRD patterns of the catalysts (grained or deposited on supports). Identified phases: A – TiO<sub>2</sub> anatase, C – Co<sub>3</sub>O<sub>4</sub> oxide, S – stainless steel support, (a) – K/Co<sub>3</sub>O<sub>4</sub>-grains, (b) – K/Co<sub>3</sub>O<sub>4</sub>/TiO<sub>2</sub>-pellets, (c) – K/Co<sub>3</sub>O<sub>4</sub>/SSWM.

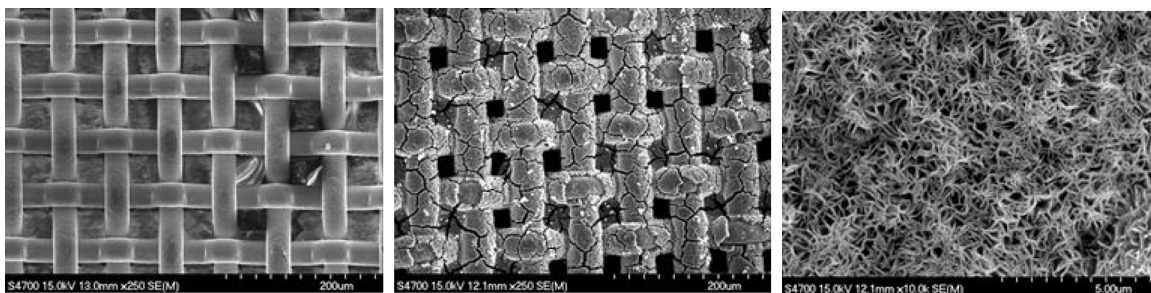


**Fig. 2.** Micrographs (SEM) of a stainless steel mesh used as a carrier for the electrochemical deposition (left), the sieve with the coated  $\text{Co}_3\text{O}_4$  (middle) and the detailed image of surface of the oxide layer (right).

phases. Three distinct diffraction lines found between  $50^\circ$  and  $60^\circ$   $2\theta$  belong to stainless steel support; these lines are characteristic for the Fe-Cr-Ni alloys (PDF #33-0397 and 35-1375). Electrochemical synthesis of precursor on the stainless steel sieve led to formation of product layer with thickness of about 7–11  $\mu\text{m}$ ; this layer consisted of thin platelet crystals preserved after calcination at  $500^\circ\text{C}$  (Fig. 2). We observed similar morphology in SEM images of Co-Mn-Al mixed oxides obtained from LDH precursors crystallized under hydrothermal conditions on anodized aluminum foils [15]. Such morphology of  $\text{Co}_3\text{O}_4$  oxide layer in the K/ $\text{Co}_3\text{O}_4$ /SSWM sample enabled easy interaction between the oxide and reducing gas. The K/ $\text{Co}_3\text{O}_4$ -grains sample consisted of grains with particle size of 160–315  $\mu\text{m}$ . Relatively big aggregates of small crystals are characteristic for the precipitated products and, moreover, such aggregates are connected during drying the filtration cake to form a rather compact material, which was subsequently calcined and crushed. Then, a different microstructure affecting reducibility of the K/ $\text{Co}_3\text{O}_4$ -grains sample in comparison with the K/ $\text{Co}_3\text{O}_4$ /SSWM one can be expected. Nearly the same crystallite sizes of  $\text{Co}_3\text{O}_4$  active phase (approximately 45 nm) was determined from the powder XRD patterns of both  $\text{Co}_3\text{O}_4$  oxide deposited on the supports and the  $\text{Co}_3\text{O}_4$  prepared in the form of grains. Electron microscopy was used to study a contact between  $\text{Co}_3\text{O}_4$  spinel, K promoter and  $\text{TiO}_2$  and SSWM supports.

STEM images show that in the case of  $\text{TiO}_2$  support, the active  $\text{Co}_3\text{O}_4$  phase is distributed on a support in the clusters form (Fig. 3). EDS analysis was performed on 3 different areas of catalysts samples. Results showed that analysis for all studied areas are identical, thus only chemical analysis of fragments 1 and 2 (Table 2) for the areas corresponding to Fig. 3 is presented. EDS maps of K/ $\text{Co}_3\text{O}_4$ / $\text{TiO}_2$  catalyst (Fig. 4) show very good dispersion of potassium on the  $\text{Co}_3\text{O}_4$  active phase and also on  $\text{TiO}_2$  support. EDS maps from K/ $\text{Co}_3\text{O}_4$ /SSWM (Fig. 5) show very good homogenization and dispersion of all elements in the catalyst.

Specific surface area SBET of the catalysts varied within the limits of 1–75  $\text{m}^2 \text{g}^{-1}$ . The highest surface area was determined for the K/ $\text{Co}_3\text{O}_4$  impregnated on  $\text{TiO}_2$  pellets, while the lowest for K/ $\text{Co}_3\text{O}_4$ /SSWM, caused very likely by higher specific density of the sieves and very thin layer of active phase covering the support. Mesopore volume of the pellets and grains was not high, 0.23 and 0.09  $\text{cm}^3 \text{g}^{-1}$ , respectively, corresponding to average radius of pores 5.1 and 18 nm, respectively. Internal diffusion in larger pores proceeds more easily and therefore, large pores are important in diffusion of reactants into the pellets interior. For that reason, mercury porosimetry of the Co impregnated  $\text{TiO}_2$  pellets was also performed. The obtained data showed pore volume about 0.48  $\text{cm}^3 \text{g}^{-1}$  and average pore radius of 41 nm. Total pore volumes and pore radii of the other two samples were not examined by mercury porosimetry, but it is very likely that pore volume of the layer of the K/ $\text{Co}_3\text{O}_4$ /SSWM sample, with respect to its small surface area, is very low.

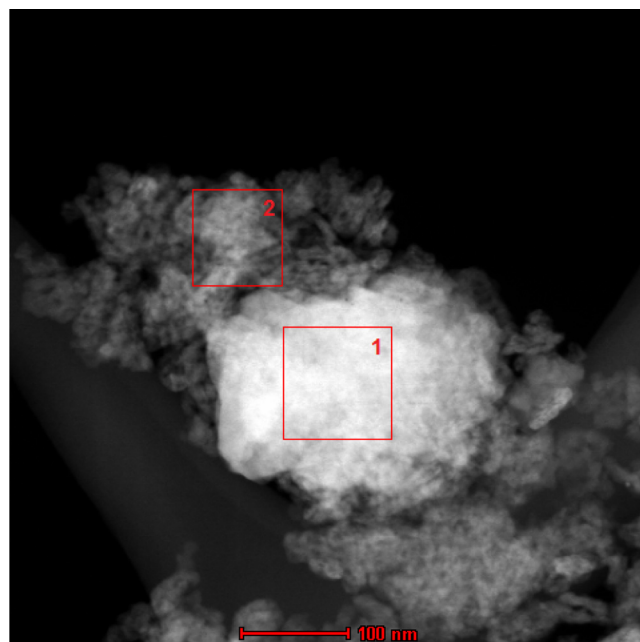


**Fig. 3.** STEM image of K/ $\text{Co}_3\text{O}_4$ / $\text{TiO}_2$ -pellets.

TPR- $\text{H}_2$  results show significant differences in the  $\text{H}_2$  consumption corresponding to the presence of different amounts of reducible species connected with different amounts of cobalt in each sample. Therefore, the obtained amounts of species reducible in the temperature range where  $\text{N}_2\text{O}$  catalytic decomposition proceeds, were recalculated in accordance with the amount of cobalt in each sample (see Table 1). Such  $\text{H}_2$  consumptions are closer to each other; the K/ $\text{Co}_3\text{O}_4$ /SSWM catalyst contained slightly higher amount of reducible species per mol of cobalt. From TPR profiles (Fig. 6) we can see that reduction of K/ $\text{Co}_3\text{O}_4$  deposited on sieves proceeds in one-step with  $T_{\text{max}}$  around  $360^\circ\text{C}$  while two peaks are clearly visible in TPR profiles of K/ $\text{Co}_3\text{O}_4$  grains (312 and  $416^\circ\text{C}$ ). The sample K/ $\text{Co}_3\text{O}_4$  deposited on  $\text{TiO}_2$  tablets showed temperature maximum at  $422^\circ\text{C}$ . Influence of addition of potassium in the TPR graphs manifests itself as a second maximum (K/ $\text{Co}_3\text{O}_4$ -grains) or shoulder (K/ $\text{Co}_3\text{O}_4$ / $\text{TiO}_2$ -pellets and K/ $\text{Co}_3\text{O}_4$ /SSWM) at lower temperatures. According to reported data, the reduction of  $\text{Co}^{3+}$  to  $\text{Co}^{2+}$  proceeds in the lower temperature region and reduction of  $\text{Co}^{2+}$  to  $\text{Co}^0$  at temperatures higher than  $400^\circ\text{C}$  [16,17]. Relative portions of both reduction processes depend on dispersion of respective active phases. Influence of stronger interaction between  $\text{Co}_3\text{O}_4$  spinel phase and  $\text{TiO}_2$  ( $\text{CoTiO}_3$ ) [18] is manifested in the form of the second shoulder at  $473^\circ\text{C}$ . Sample of K/ $\text{Co}_3\text{O}_4$ /SSWM before TPR analysis was cut on the small piece about 1 mm, samples of K/ $\text{Co}_3\text{O}_4$ -grains and K/ $\text{Co}_3\text{O}_4$ / $\text{TiO}_2$ -pellets were measured in grains

**Table 2**  
Quantitative EDS analysis of K/Co<sub>3</sub>O<sub>4</sub>/TiO<sub>2</sub>-pellets.

	Co		Ti		K		O	
	wt.%	Uncert.%	wt.%	Uncert.%	wt.%	Uncert.%	wt.%	Uncert.%
Fragment 1	52	0.23	17	0.12	0.4	0.02	30.6	0.23
Fragment 2	1.4	0.08	54	0.38	0.5	0.04	44.1	0.52

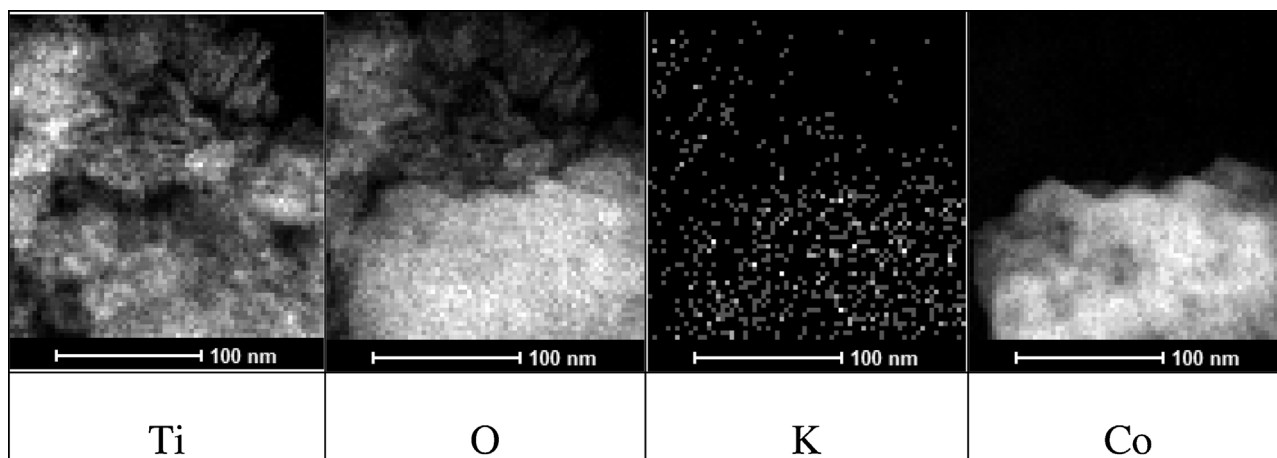


**Fig. 4.** EDS maps of of K/Co<sub>3</sub>O<sub>4</sub>/TiO<sub>2</sub>-pellets.

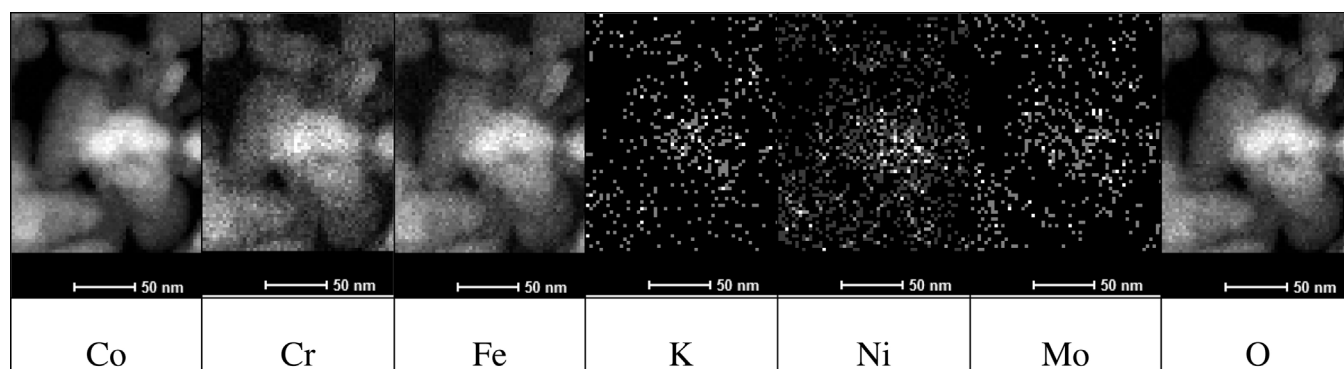


**Fig. 5.** EDS maps of of K/Co<sub>3</sub>O<sub>4</sub>/SSWM.

form with particle size 0.316–0.165 mm. It was found out that the deposition of K/Co<sub>3</sub>O<sub>4</sub> active layer on TiO<sub>2</sub> support led to the formation of clusters of Co<sub>3</sub>O<sub>4</sub> crystallites compared to wire mesh support where homogeneous distribution of Co<sub>3</sub>O<sub>4</sub> crystallites was observed, which could also contribute to the worse reducibility of K/Co<sub>3</sub>O<sub>4</sub> deposited on TiO<sub>2</sub> compared to wire mesh catalyst. Layer of active phase deposited on the sieve is almost 25 times smaller than size of grains and lack of internal diffusion during TPR measurement in thin catalyst layer on the sieve can explain that main maximum is shifted to lower temperature (360 °C).

### 3.2. N<sub>2</sub>O catalytic decomposition

Three kinds of the prepared K/Co<sub>3</sub>O<sub>4</sub>-based catalysts were tested in laboratory reactors under defined conditions (Fig. 7). However, the temperature dependences of N<sub>2</sub>O conversions depicted in Fig. 7 cannot be directly compared because of different mean residence time caused by differences in catalysts size and possibilities of our experimental set-up. Therefore, the obtained catalytic data were used for evaluation of specific activity expressed as quasi-turnover frequency (QTOF), which can tell us, how many moles of N<sub>2</sub>O decompose on the same amount of cobalt used for

catalyst preparation. This is important in order to specify utilization of amount of cobalt consumed at catalyst preparation, which is closely connected with catalyst price. Mathematical model of catalytic reactor is used to enable determination of N<sub>2</sub>O conversion at same mean residence time expressed per the unit volume of catalyst bed, which means comparison on the basis of volume of the catalyst that can be filled in the same volume of the deN<sub>2</sub>O catalytic reactor. The QTOF was calculated according to Eq. (1):

$$QTOF = \frac{p_{atm} X_{N_2O} X_{N_2O} VM}{m w_{Co} RT} \quad (\text{mol}_{N_2O} \text{ s}^{-1} \text{ g}_{Co}^{-1}) \quad (1)$$

Temperature dependence of QTOF is shown in Fig. 8a. Except different amounts of active Co species in the prepared catalysts, tested samples contained also slightly different amounts of potassium promoter. It was found out previously that catalytic activity for N<sub>2</sub>O decomposition in inert gas is dependent on the K/Co molar ratio reaching maximum at value of K/Co from 0.04 to 0.06 [19] which is little higher than K/Co ratio determined in catalysts prepared in presented work. Then an increase in N<sub>2</sub>O conversion is possible by potassium content increase to optimal level. According to the K/Co ratios in our samples (see Table 1), one can suppose that K/Co<sub>3</sub>O<sub>4</sub>-grains and K/Co<sub>3</sub>O<sub>4</sub>-pellets should possess higher specific

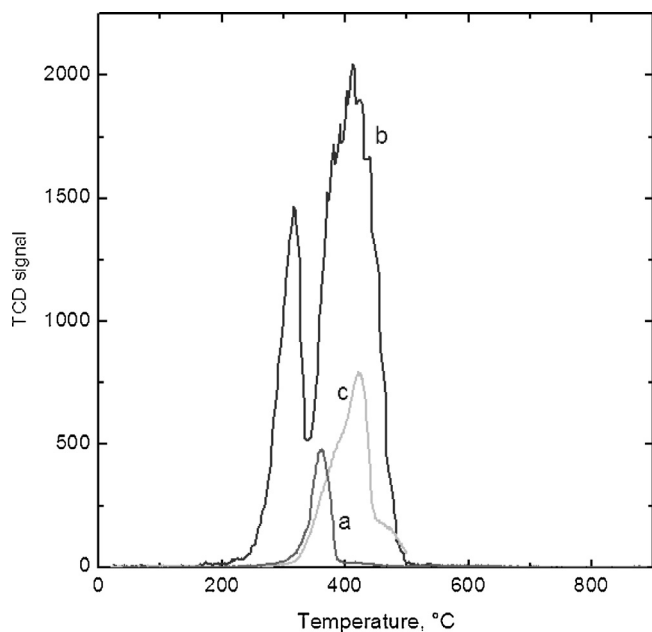


Fig. 6. TPR-H<sub>2</sub> profiles of prepared catalysts: (a) K/Co<sub>3</sub>O<sub>4</sub>/SSWM, (b) K/Co<sub>3</sub>O<sub>4</sub>\_grains, (c) K/Co<sub>3</sub>O<sub>4</sub>/TiO<sub>2</sub>\_pellets.

activity than that obtained over the K/Co<sub>3</sub>O<sub>4</sub> deposited on SSWM. However, calculated QTOF values did not follow this trend. The highest specific activity was obtained over K/Co<sub>3</sub>O<sub>4</sub> deposited on the sieve at high reaction temperatures, while at lower temperatures; the QTOF values were comparable with grained K/Co<sub>3</sub>O<sub>4</sub>. In this case the QTOF value gives us information about the utilizability of the cobalt used for catalyst preparation – sample with higher QTOF could contain less cobalt in order to reach the same N<sub>2</sub>O conversion, and is thus less expensive. Much lower value of QTOF calculated for K/Co<sub>3</sub>O<sub>4</sub>/TiO<sub>2</sub>\_pellets can be explained by the influence of internal diffusion on the rate of N<sub>2</sub>O decomposition. To confirm this assertion, a resistance to internal diffusion ( $1/\eta$ , where  $\eta$  is internal effectiveness factor) in these catalysts was calculated according to Eqs. (2)–(7) [20–22], using the kinetic constant ( $k = k_0 e^{-E_A/RT}$ ,  $k_0 = 127.7 \times 10^4 \text{ m}^3 \text{ g}^{-1} \text{ s}^{-1}$ ,  $E_A = 132893 \text{ J mol}^{-1}$ ) evaluated from kinetic data on the K/Co<sub>3</sub>O<sub>4</sub> grains. Internal effectiveness factor was calculated according to relation valid for first-order reaction in a spherical catalyst pellet [20]:

$$\eta = \frac{3}{\Phi^2} (\Phi \coth \Phi - 1) \quad (2)$$

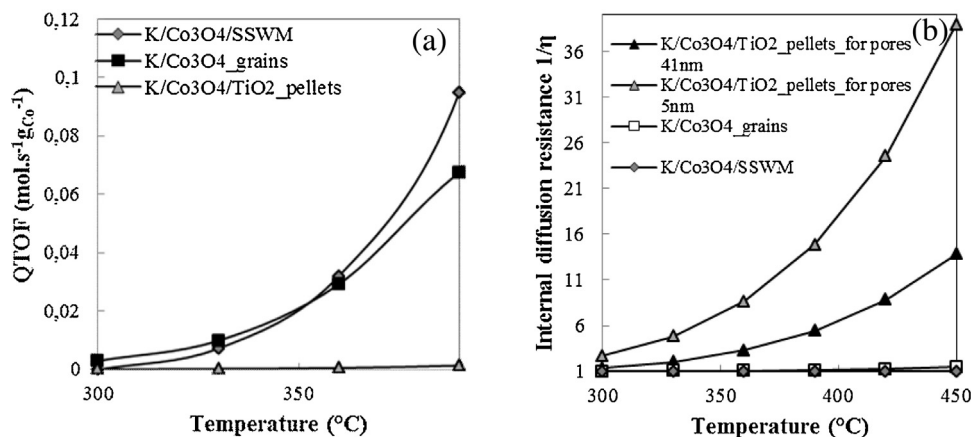


Fig. 8. Temperature dependence of QTOF (a) and internal diffusion resistance  $1/\eta$  (b) of K/Co<sub>3</sub>O<sub>4</sub> in powder form, K/Co<sub>3</sub>O<sub>4</sub> deposited on stainless steel sieves and K/Co<sub>3</sub>O<sub>4</sub> deposited on TiO<sub>2</sub> pellets.

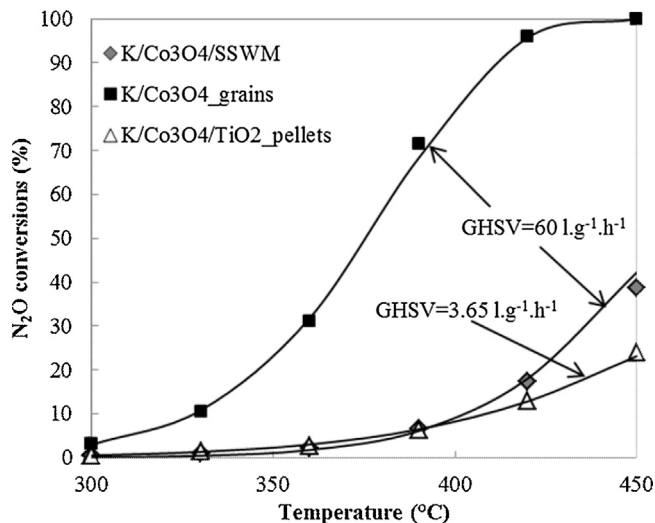


Fig. 7. Temperature dependence of N<sub>2</sub>O conversions over K/Co<sub>3</sub>O<sub>4</sub> catalysts in laboratory reactor, points – experimental data, lines – model. Conditions: inlet concentration of N<sub>2</sub>O 0.1 mol% in N<sub>2</sub>.

where Thiele module  $\Phi$  is defined as [20]:

$$\Phi = r_p \sqrt{\frac{k \cdot \rho_c}{D_{\text{eff}}}} \quad (3)$$

For estimation of effective diffusion coefficient  $D_{\text{eff}}$ , value of ratio  $\varepsilon_p/q = 1$  was used [21]:

$$D_{\text{eff}} = \frac{\varepsilon_p \bar{D}}{q} \quad (4)$$

$$\frac{1}{D} = \frac{\alpha_i}{D_{ki}} + \sum_{j=1}^p \frac{\alpha_i x_j + \alpha_j x_i}{D_{ij}} + \alpha_i \sum_{j=q}^n \frac{x_i}{D_{ij}} \quad (5)$$

$$D_k = 97 \cdot r_0 \cdot \sqrt{\frac{T}{M_{\text{N}_2\text{O}}}} \quad (6)$$

$$D_{ij} = \frac{10^{-4} T^{7/4} (M_j^{-1} + M_i^{-1})^{1/2} / p}{\left[ (\sum v_i)^{1/3} + (\sum v_j)^{1/3} \right]^2} \quad (7)$$

Temperature dependence of the resistance to internal diffusion in the prepared catalysts is plotted in Fig. 8b). For pelletized catalyst, the internal diffusion resistance was calculated for limiting situations, it means if there are present mesopores with radius of pores only 5 nm or only with 41 nm (see Table 1). The real value

**Table 3**Input parameters for the model of reactor for the N<sub>2</sub>O catalytic decomposition over K/Co<sub>3</sub>O<sub>4</sub> supported on TiO<sub>2</sub> tablets and SSWM.

K/Co <sub>3</sub> O <sub>4</sub> /SSWM		K/Co <sub>3</sub> O <sub>4</sub> /TiO <sub>2</sub> -tablets	
The total area of sieves per 1 m <sup>3</sup> of catalyst bed (m <sup>2</sup> )	88	Equivalent diameter of the catalyst tablets 5 mm × 5 mm (m)	0.00527
Gap between sieves (mm)	0.5	Porosity of the catalyst bed (-)	0.529
Amount of Co per 1 m <sup>3</sup> of catalyst bed (kg)	0.0591	Amount of Co per 1 m <sup>3</sup> of catalyst bed (kg)	6.31
Activation energy (J/mol)	153 000	Activation energy (J/mol)	96 000
Pre-exponential factor $k_0$ (m <sup>3</sup> m <sup>-2</sup> s <sup>-1</sup> )	$4.2 \times 10^8$	Pre-exponential factor $k_0$ (m <sup>3</sup> m <sup>-3</sup> s <sup>-1</sup> )	4.6
Pressure at the reactor inlet (Pa)	600 000	Pressure at the reactor inlet (Pa)	60 000
Temperature (°C)	330–450	Temperature (°C)	330–450
GHSV <sup>a</sup> (m <sup>3</sup> <sub>gas</sub> h <sup>-1</sup> m <sup>3</sup> <sub>bed</sub> )	10 909	GHSV <sup>a</sup> (m <sup>3</sup> <sub>gas</sub> h <sup>-1</sup> m <sup>3</sup> <sub>bed</sub> )	10 909
Superficial gas velocity (m s <sup>-1</sup> )	1.9	Superficial gas velocity (m s <sup>-1</sup> )	1.9

<sup>a</sup> Reactor was modeled with internal diameter 30 cm and length of the catalyst bed 63 cm, total gas flow 600 kg/min was used.

of internal diffusion resistance will be of course somewhere in the mentioned region. Increasing value of the resistance to internal diffusion,  $1/\eta$ , means increasing limitation of reaction rate by internal mass transfer; value of one represents no internal diffusion limitation. It is seen that there was a high effect of internal diffusion inside the tablets and only small contribution of the internal diffusion effects in the K/Co<sub>3</sub>O<sub>4</sub> grains at higher temperatures. Catalyst layer on the sieve is so thin (7–11 μm) that we can neglect the influence of the internal diffusion on the reaction rate ( $1/\eta = 1$ ).

On the basis of internal diffusion limitations, the K/Co<sub>3</sub>O<sub>4</sub> stainless steel wire mesh catalyst combines suitable features of active cobalt species with the effective utilization of all active components disposed in the catalyst. To confirm the promising characteristics of the K/Co<sub>3</sub>O<sub>4</sub> supported on the SSWM, the mathematical model of catalytic reactor based on laboratory data was used for calculations of N<sub>2</sub>O conversions per unit volume of catalyst bed composed from K/Co<sub>3</sub>O<sub>4</sub>/SSWM or K/Co<sub>3</sub>O<sub>4</sub>/TiO<sub>2</sub>-pellets and a comparison on the basis of volume of the catalyst that can be filled in the known volume of the deN<sub>2</sub>O catalytic reactor is performed.

### 3.3. Mathematical model of the catalytic reactor for N<sub>2</sub>O decomposition

A pseudo-homogeneous one-dimensional model of an ideal plug flow reactor in an isothermal regime was used for the reactor simulation (Eqs. (8)–(16)). The influence of internal and external heat transfer on the reaction rate was neglected as well as effect of external mass transfer. The verification of the model based on laboratory experiments was done previously [22]; comparison of the measured and calculated data in laboratory reactor is shown in Fig. 7. The mathematical model consists of the following equations:

Mass balance of N<sub>2</sub>O in dV [22]:

$$\alpha_A \cdot r \cdot \frac{dV}{\dot{V}} = dC_A \quad (8)$$

The kinetic equation assuming the 1st order reaction rate:

$$r = k \cdot C_A \quad (9)$$

Arrhenius equation:

$$k = k_0 e^{-E_A/RT} \quad (10)$$

The concentration of N<sub>2</sub>O expressed in terms of conversion  $X_A$ , assuming that the change of the total volumetric flow rate due to N<sub>2</sub>O decomposition is negligible:

$$C_A = (C_{A0} - X_A \cdot C_{A0}) \cdot \frac{p}{p_0} \quad (11)$$

Pressure drop in gas flow through the catalyst bed in the form of tablets:

$$\frac{dp}{dz} = - \frac{2 \cdot v^2 \cdot C_D \cdot \rho}{dp} \quad (12)$$

$$C_D = \frac{1 - \varphi}{\varphi^3} \cdot \left( \frac{150 \cdot (1 - \varphi)}{Re'} + 1.75 \right) \quad (13)$$

$$Re' = \frac{\varphi \cdot g_c \cdot d_p \cdot \dot{V}}{S \cdot \mu} \quad (14)$$

Pressure drop in the reactor with a catalyst deposited on the sieve [23]:

$$p = p_0 - \Delta p \cdot n \quad (15)$$

$$\Delta p = \frac{m^2 \cdot (1 - (A_f/A_p)^2)}{C^2 \cdot A_f^2 \cdot 2 \cdot \rho} \quad (16)$$

where  $A_p$  is surface of one sieve ( $A_p = 0.07065 \text{ m}^2$ ),  $A_f$  is surface of holes in one sieve ( $A_f = 0.0127 \text{ m}^2$ ).

It was supposed that whole reactor is filled with the chosen catalyst which means that different weight of catalyst and also different weight of cobalt could be placed inside the reactor. The parameter which was set as a constant for both simulations was the volume of the reactor. For the catalyst deposited on a sieve, the reactor was modeled as a reactor with a catalyst in the form of sieves, which are stacked one on the other with gap of 0.5 mm between them. For modeling of reactor with catalyst in the form of tablets, the model of fixed bed reactor was used. Input parameters of the model for the N<sub>2</sub>O catalytic decomposition reactor are shown in Table 3, the GHSV, temperature and pressure corresponding to the conditions in HNO<sub>3</sub> commercial production units were used.

Calculated N<sub>2</sub>O conversions and pressure drop for both type of supported catalysts are depicted in Fig. 9. Obtained values of N<sub>2</sub>O conversion look very promising, since significantly higher conversions were achieved over K/Co<sub>3</sub>O<sub>4</sub> deposited on the SSWM than over tablets in spite of the fact that the total amount of cobalt per unit volume of bed was 100 times lower than in the case of the tablets. It is known that structured catalysts on the base of monolith and sieves generally guarantee lower pressure drop than fixed bed of pellets and good heat transfer through the reactor. In our model reactor, the structured fixed bed of wire mesh has larger pressure drop than classical fixed bed of the pellets, but this difference is too small to affect the calculated N<sub>2</sub>O conversion and has to be a subject of further optimization. The thickness of the wall of a wire mesh and diameter of the hole must be chosen according to process condition since the diameter of hole determines the pressure drop. In this work, the stainless steel sieves with a mesh size of 40 μm were studied, which are suitable for laboratory tests. Other parameter which can also be optimized is gas velocity, and can be decreased by increasing the reactor diameter.

Deposition of the active phase on high surface support can generally increase interface between gas and solid surface, however our calculation showed that in present case this effect is considerably masked by the internal diffusion limitations occurring in the pores of tablets. Advantages of promoters, doping and other effects

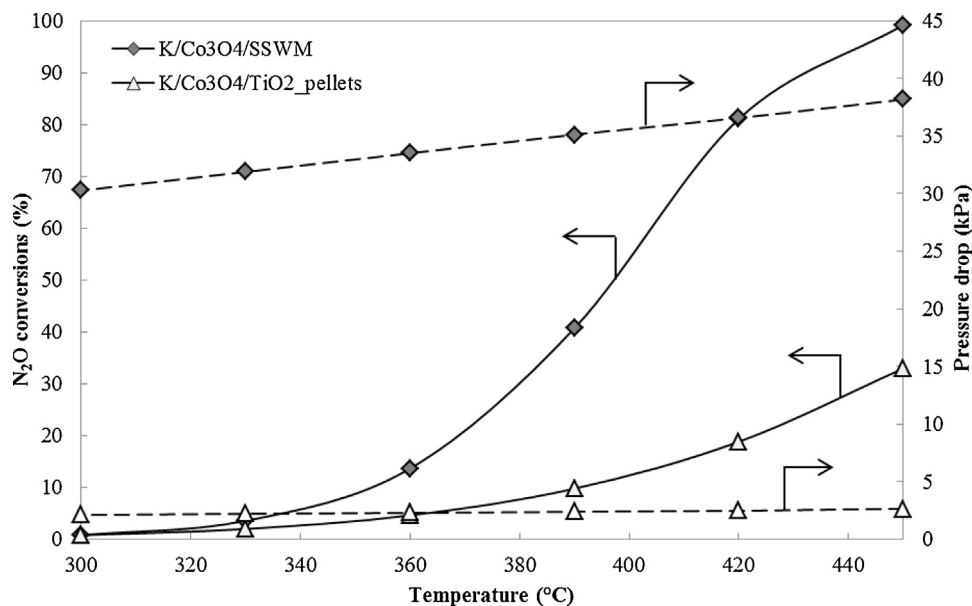


**Fig. 9.** Comparison of the calculated temperature dependences of N<sub>2</sub>O conversion and pressure drop (kPa) over K/Co<sub>3</sub>O<sub>4</sub> supported on TiO<sub>2</sub> pellets and SSWM at GHSV = 10 909 m<sup>3</sup> h<sup>-1</sup> m<sub>bed</sub><sup>-3</sup>.

evident in laboratory conditions lose their significance if the internal diffusion limitations are not absent. Stainless steel wire mesh represents support which can overcome this limitation and we confirmed that deposition of the K/Co<sub>3</sub>O<sub>4</sub> active phase on the SSWM instead of porous TiO<sub>2</sub> tablets bring a huge saving of amount of cobalt deposited on the catalyst.

#### 4. Conclusions

K/Co<sub>3</sub>O<sub>4</sub> supported on two different supports – stainless steel wire mesh and TiO<sub>2</sub> tablets were prepared to compare advantage and disadvantage of porous and non-porous supports. Prepared catalysts were characterized and tested for N<sub>2</sub>O catalytic decomposition. For comparison, K/Co<sub>3</sub>O<sub>4</sub> grains were used.

Despite of more than seventy times higher surface area, five times higher content of active cobalt spinel phase and almost optimal content of K promoter in the K/Co<sub>3</sub>O<sub>4</sub> supported on TiO<sub>2</sub>, higher N<sub>2</sub>O conversion per unit of catalyst bed was calculated (using simple mathematic model of catalytic plug flow reactor) for K/Co<sub>3</sub>O<sub>4</sub> supported on stainless steel wire mesh. The reason is that all above mentioned advantages of K/Co<sub>3</sub>O<sub>4</sub> supported on porous TiO<sub>2</sub> were covered by hindering effect of internal diffusion in TiO<sub>2</sub> pores which caused decrease of overall reaction rate of N<sub>2</sub>O decomposition. Higher N<sub>2</sub>O conversion reached on the same volume of catalyst bed showed that stainless steel sieves have high potential for practical application. They provide appropriate conditions for obtaining active catalysts, in which the negative effects of internal diffusion are minimized and the active components are effectively utilized.

#### Acknowledgements

This work was supported by the Czech Science Foundation (project 14-13750S), by Ministry of Education, Youth and Sports of the Czech Republic in National Feasibility Program I (project “TEWEP” LO1208) and VŠB-TU student projects SP2014/48 and

SP2015/125. Kateřina Mamulová-Kutláková from Nanotechnology Centre VŠB-TU is acknowledged for XRD measurements.

#### References

- [1] J. Pérez-Ramírez, F. Kapteijn, K. Schoffel, J.A. Moulijn, *Appl. Catal. B* 44 (2003) 117–151.
- [2] Li Xuea, Changbin Zhanga, Hong Hea, Yasutake Teraoka, *Appl. Catal. B: Environ.* 75 (2007) 167–174.
- [3] K. Asano, Ch. Ohnishi, S. Iwamoto, Y. Shioya, M. Inoue, *Appl. Catal. B: Environ.* 78 (2008) 242–249.
- [4] B.M. Abu-Zied, S.A. Soliman, S.E. Abdellah, *Chin. J. Catal.* 35 (2014) 1105–1112.
- [5] L. del Río, G. Marbán, *Appl. Catal. B* 126 (2012) 39–46.
- [6] L. Obalová, K. Karásková, A. Wach, P. Kustrowski, K. Mamulová-Kutláková, S. Michalík, K. Jiráťová, *Appl. Catal. A: Gen.* 462–463 (2013) 227–235.
- [7] L. Obalová, G. Maniak, K. Karásková, F. Kovanda, A. Kotarba, *Catal. Commun.* 12 (2011) 1055–1058.
- [8] M. Inger, M. Wilk, M. Saramok, G. Grzybek, A. Grodzka, P. Stelmachowski, W. Makowski, A. Kotarba, Z. Sojka, *Ind. Eng. Chem. Res.* 53 (25) (2014) 10335–10342.
- [9] M. Inger, P. Kowalik, M. Saramok, M. Wilk, P. Stelmachowski, G. Maniak, P. Granger, A. Kotarba, Z. Sojka, *Catal. Today* 176 (2011) 365–368.
- [10] L. del Río, G. Marbán, *Appl. Catal. B* 150–151 (2014) 370–379.
- [11] K. Karásková, L. Obalová, F. Kovanda, *Catal. Today* 176 (2011) 208–211.
- [12] A. Klyushina, K. Pacultová, L. Obalová, *Reac. Kinet. Mech. Cat.* (2015), <http://dx.doi.org/10.1007/s11144-015-0871-y>
- [13] P. Stelmachowski, G. Maniak, A. Kotarba, Z. Sojka, *Catal. Commun.* 10 (2009) 1062–1065.
- [14] Z.P. Xu, H.C. Zeng, *Int. J. Inorg. Mater.* 2 (2000) 187–196.
- [15] F. Kovanda, K. Jiráťová, J. Ludvíková, H. Raabová, *Appl. Catal. A* 464–465 (2013) 181–190.
- [16] G. Maniak, P. Stelmachowski, A. Kotarba, Z. Sojka, V. Rico-Perez, A. Bueno-Lopez, *Appl. Catal. B* 136–137 (2013) 302–307.
- [17] M. Sun, L. Wang, B. Feng, Z. Zhang, G. Lu, Y. Guo, *Catal. Today* 175 (2011) 100–105.
- [18] M.M. Yung, E.M. Holmgren, U.S. Ozkan, *J. Catal.* (2007) 356–367.
- [19] L. Obalová, K. Karásková, K. Jiráťová, F. Kovanda, *Appl. Catal. B* 90 (2009) 132–140.
- [20] H.S. Fogler, *Elements of Chemical Reaction Engineering*, 3rd ed., Prentice Hall PTR, New Jersey, 1999.
- [21] F. Kapteijn, J.A. Moulijn, G. Ertl, H. Knözinger, J. Weitkamp (Eds.), *Handbook of Heterogeneous Catalysis*, vol. 3, 1996, pp. 1359–1376.
- [22] L. Obalová, K. Jiráťová, K. Karásková, F. Kovanda, *Chin. J. Catal.* 32 (2011) 816–820.
- [23] O. Švec, <http://chps.fsid.cvut.cz/pt/2011/pdf/1100013-1.pdf> (accessed 31.10.14).